Pre-print: L. Gurreri, A. Filingeri, M. Ciofalo, A. Cipollina, M. Tedesco, A. Tamburini, G. Micale, *Electrodialysis with asymmetrically profiled membranes: influence of profiles geometry on desalination performance and limiting current phenomena*, Desalination, 506 (2021) 115001, https://doi.org/10.1016/j.desal.2021.115001

Electrodialysis with asymmetrically profiled membranes: influence of profiles geometry on desalination performance and limiting current phenomena

Luigi Gurreri[a], Antonia Filingeri[a], Michele Ciofalo[a], Andrea Cipollina[a]*, Michele Tedesco[b], Alessandro Tamburini[a], Giorgio Micale[a]

[a] *Dipartimento di Ingegneria, Università degli Studi di Palermo, viale delle scienze ed. 6, 90128 Palermo*

[b] *Wetsus, European Centre of Excellence for Sustainable Water Technology, Oostergoweg 9, 8911 MA Leeuwarden, the Netherlands*

*corresponding author – email: andrea.cipollina@unipa.it

ABSTRACT

Electrodialysis (ED) has recently gained much attention in the wide field of desalination and water treatment. However, energy consumption and capital costs may impair the process competitiveness. In this regard, limiting current density (LCD) and current efficiency (η) are key performance parameters for optimized ED systems. In this work, an experimental campaign was carried out characterizing the performance of ED stacks when adopting asymmetrically profiled membranes. Current–voltage curves were recorded under different operating conditions mimicking the operation of brackish water or seawater desalination units. Results showed that there was a preferable direction of the electric current relative to the membrane profiles, which provided higher values of LCD and of maximum η. Stacks with Overlapped Crossed Filaments profiled membranes performed better than conventional ED stacks with flat membranes and spacers by increasing the LCD (by ~20% under various operating conditions) and the maximum η (e.g. from ~55–65% to ~70–73% at 0.5-60 g/l inlet concentrations). The specific energy consumption was significantly reduced (even more than 50%). On the contrary, the investigated pillar-profiled membranes exhibited the worst performances. The

present results suggest that well-designed profiled membranes can reduce the costs of desalination via ED.

Keywords: ion exchange membrane; corrugated membrane; current utilization; polarisation phenomena; mass transport.

1 Introduction

Electrodialysis (ED) is an electro-membrane process that exploits the selective transport of ions through ion-exchange membranes under the effect of an applied electric field in order to produce two streams at different concentration [1–3]. Figure 1 reports a schematic representation of an ED unit, composed by a stack of alternated cation- and anion-exchange membranes (CEMs and AEMs), between which the solutions flow. The cell pair represents the repeating unit of the stack and consists of a CEM, an AEM, a diluate and a concentrate compartment. The stack is enclosed between two electrode chambers. An external power supply connected to the electrodes establishes an electric field inducing an ionic current through the stack. Cations, like Na^+, migrate towards the cathode, moving freely through the nearest CEM and being blocked by the AEM. *Vice versa*, anions, like Cl^-, migrate towards the anode, moving freely through the nearest AEM and being blocked by the CEM. The counter-ion transport and the co-ion block result in a salt depletion in one compartment, i.e. the diluate, and a salt enrichment in the other compartment, i.e. the concentrate.

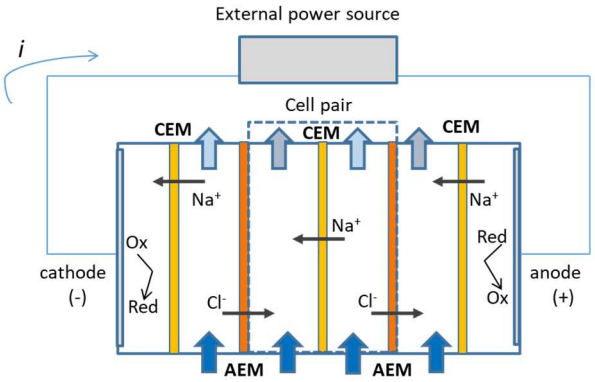

Figure 1. Schematic representation of an ED stack (adapted from [4]).

A number of different configurations of ED units have been studied for applications in food processing, biotechnology, and pharmaceutical industry [5–7]. Many studies have been conducted on the treatment of wastewater from several sources [8]. However, the main industrial application of ED is saline water desalination. ED covers ~2% of the global desalination capacity, with low to medium size plants (capacity typically below 10,000 m^3/day) [9,10] and electrical energy consumption in the range 2-5 kWh/m^3 [11]. ED has gained a main role in the market of brackish water desalination, where the small desalination rate required makes ED competitive compared to Reverse Osmosis (RO). There are some applications of ED to treat seawater for table salt production [3]. However, drinking water production from seawater is not yet competitive, thus only pilot plants have been so far installed and operated [12]. High costs are due to the loss of selectivity encountered with high concentration gradients and to the higher membrane area [13]. On the other hand, research is currently addressing the challenge of developing competitive ED systems for the desalination of concentrated solutions (e.g. brines [8]). In particular, both modelling [14–17] and experimental [18–20] studies have been conducted on ED desalination of seawater. The use of multi-stage ED systems with a suitable distribution of membrane area (decreasing in consecutive stacks) allowed for a reduction of the energy consumption up to 2.2 kWh/m^3 for desalinating a 0.51 M NaCl solution to 0.0054 M [20]. This promising result was obtained by using membranes with low permeability to water and operating at current densities up to 95% of the LCD, thus increasing current efficiency and water recovery.

Current efficiency (η) and limiting current density (LCD) are key operating parameters of ED stacks. The current efficiency depends on the selectivity and transport properties of the membranes, and is affected by salt back-diffusion and water flux via osmosis and electro-osmosis [21–24]. LCD depends on the transport mechanisms in solution (especially in the diluate compartment) and in membrane [1,25,26]. Both η and LCD are significantly affected by the channel geometry. The existence of the LCD is strongly linked to concentration polarization phenomena [27], which consist in concentration gradients developing along the channels across the boundary layer perpendicular to the membrane.

They arise from the different ions mobility between the membrane and the solution. This results in a depletion of concentration in the diluate and an enrichment of concentration in the concentrate, from the solution bulk to the solution-membrane interface [28]. As the electric current increases, the salt depletion can occur until reaching (theoretically) a null concentration at the interface. This condition provides a diffusion-limited current density, which can be estimated based on the Nernst film theory [29–31]. In the simple case of a binary electrolyte, it can be written as [1]:

$$LCD = \frac{z_i F Sh D}{d_{eq} (t_{IEM,i} - t_i)} C_{bulk,i} \quad (1)$$

where the subscript i indicates one ionic species (i.e. either anion or cation), z_i is the valence, F is the Faraday constant, Sh is the Sherwood number (mass transfer characteristics in the diluate), D is the salt diffusion coefficient in the solution, d_{eq} is the equivalent diameter (e.g. twice the channel thickness, $2H$), $t_{IEM,i}$ and t_i are the transport numbers in membrane and solution, respectively, and C_{bulk} is the bulk concentration in the diluate compartment. Despite the LCD expressed by eq. (1) defines a theoretical limiting value, a typical current–voltage curve exhibits three regions [1,3] (Figure 2), where experimentally an overlimiting condition is reached due to other phenomena sustaining a current density higher than the LCD [28,32]. This deviation from the theory applies both for simple systems, e.g. one membrane in contact with two solutions, and for ED stacks [33–36].

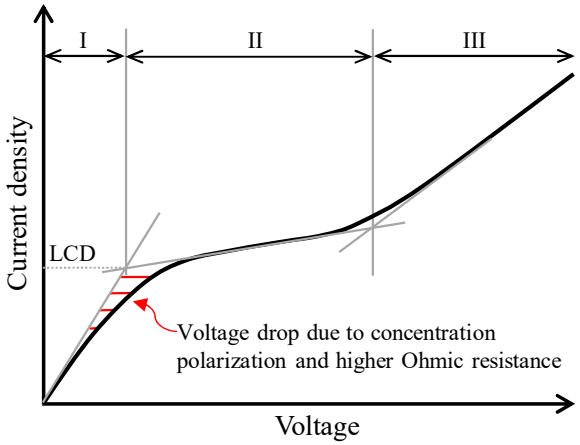

Figure 2. Current density–voltage curve of ED stacks (adapted from [1]).

Overlimiting currents can be explained only partially by the formation of charge carriers via water dissociation (H^+ and OH^-) [37,38]. Electroconvection, instead, can be the main overlimiting mechanism involving the transport of salt ions [28,39,40]. Non-equilibrium electroconvection occurs through the development of an extended space charge region near the membrane and inhomogeneous electric fields causing dynamic vortices [41–44]. Overlimiting mechanisms and *i–V* curves are affected by membrane surface properties, such as the heterogeneity of conductivity and surface geometry [45–49], as well as roughness, grade of hydrophobicity, and superficial charge density [25,32,50,51].

The understanding of phenomena affecting LCD and the *i–V* behaviour is of fundamental importance to prevent the drastic increase of the stack resistance and water dissociation that can lead to scaling or fouling. Moreover, stacks and operating conditions providing higher LCD values offer the possibility of desalinating with reduced membrane area and, thus, reduced investment costs [3]. The LCD is conventionally assumed as a practical threshold for operating ED units. On the other hand, recent studies have focused on overlimiting regimes enhancing mass transfer [39,52]. In all cases, the LCD and the limiting behaviour of the stack are crucial to enhance the process efficiency.

Stack design and membrane surface properties affect the LCD in ED, and novel stack and IEM designs can be exploited to enhance the ED performance in the limiting region. In this regard, a promising ED development is the use of profiled (or corrugated) membrane, which allow ED stacks to be assembled without separated spacers. Profiled membranes are provided with ion conductive ridges, pillars or reliefs, designed to create the solution compartment [1,3]. Depending on the profiles shape and on the operating conditions, profiled membranes may lead to several advantages over conventional configurations with flat membranes and spacers [53]: lower electrical resistance, higher active area, lower water splitting thanks to lower local current densities [28], reduction of concentration polarization and increase of LCD (when proper geometries enhancing mixing are

adopted), facilitation of electroconvection, lower fouling sensibility (compared to conventional spacers [54]), and lower pressure drop.

Larchet et al. [52] showed that profiled membranes increased mass transfer in ED units operated at high electric currents (including overlimiting currents), resulting in a larger range of inlet concentration in which high desalination rates were obtained, and reduced the hydraulic resistance. Strathmann [3] reported ED experiments performed with profiled membranes with trapezoidal cross-section profiles, which increased the active area by over 40%. The stack with profiled membranes exhibited lower resistances and higher LCDs, yielding a higher desalination rate at any voltage. Balster et al. [55] found an increase of LCD of more than 30% and a reduction of electrical resistance by using profiled membranes. Zhao et al. [56] tested different notched membranes, which exhibited higher desalination rates and a LCD increase of up to three times. Melnikov et al. [57] tested profiled membranes in ED for the desalination of secondary steam condensate from ammonium nitrate production. The stack with profiled membranes provided higher values of η and LCD, while suppressing water dissociation [57]. Pressure drop is strongly affected by the profiles geometry, and both experiments [58] and simulations [59] showed that the hydraulic resistance may be reduced by simple profile-filled channels. Numerical simulations based on mathematical models confirmed the possibility to enhance the process performance by using profiled membranes [60,61].

Despite the increasing interest in profiled membranes for ED, the effect of profile geometry on LCD is still unknown. The aim of this work is to assess the performance of ED systems equipped with profiled membranes of different geometry, and quantify the effects on LCD and desalination performance. Current–voltage characteristics were recorded under different operating conditions mimicking both brackish water and seawater (limiting the analysis to the final stage of the process) desalination conditions. Different profiling geometries were used, namely membranes with Overlapped Crossed Filament profiles and with Pillar profiles, using conventional flat membranes for

comparison purposes. In all cases, the performance of the ED system was evaluated in terms of current efficiency (η), LCD, and energy consumption.

2 Experimental

The present experimental campaign consisted of single-pass ED tests with lab-scale stacks equipped either with profiled membranes or with conventional "flat" membranes and spacers. In particular, current–voltage (*i*–*V*) curves were recorded in order to characterize the various ED stacks under different operating conditions (inlet concentrations, fluid velocity and relative arrangement of the profiles with respect to the direction of the electric current) mimicking seawater or brackish water desalination with artificial NaCl solutions. At each applied current, the data collected were voltage and outlet concentrations. The limiting current density was identified from the *i*–*V* curve. Current efficiency and specific energy consumption were calculated.

2.1 Materials and set-up

The experimental campaign was carried out with a lab-scale ED stack (REDstack BV, The Netherlands) composed of 10 cell pairs with active area of 10×10 cm^2 and characterized by cross-flow layout of diluate and concentrate solutions. Fujifilm Type-10 CEM/AEM (Fujifilm Manufacturing Europe BV, The Netherlands) were used for all the tests, and the main properties are reported in Table 1. Two types of profiled membranes were used: Overlapped Crossed Filaments (OCF) and Pillars. Our research group studied similar geometries by numerical models ([62–64] for OCF profiles and [59,65] for pillar profiles). Membrane profiles were manufactured by adding ion conductive cross-linked resin on existing base membranes by a screen printing process.

Table 1. Properties of the Fujifilm Type 10 ion-exchange membranes used in this study. "n.p." means "not provided".

		Permselectivity[a] [%]	Water permeability [ml/(m² h bar)]	Salt diffusivity [m²/s]	IEC [meq/g]	Areal resistance[b] [Ω cm²]	Thickness (dry) [µm]	Thickness (wet) [µm]	Profile thickness (wet) [µm]
Flat	AEM	97	6.29	$4 \cdot 10^{-12}$	2.85	1.77	120	130	-
	CEM	98	7.79	$4 \cdot 10^{-12}$	2.9	1.89	120	130	-
OCF 270[c]	AEM	95.1	7.63	$2.7 \cdot 10^{-12}$	2.85	2.36	120	130	135
	CEM	99.5	5.26	$2.7 \cdot 10^{-12}$	n.p.	3.21	120	130	135
OCF 150[c]	AEM	94.7	5.65	$2 \cdot 10^{-12}$	n.p.	2.07	120	130	75
	CEM	99.3	5.49	$2 \cdot 10^{-12}$	n.p.	2.8	120	130	75
Pillar 155[c]	AEM	94.3	6.11	$4.3 \cdot 10^{-12}$	n.p.	1.89	120	130	155
	CEM	99	6.99	$4.3 \cdot 10^{-12}$	n.p.	2.48	120	130	155

[a] Measured between 0.05 M and 0.5 M KCl solutions at 25 °C.

[b] Measured in 2 M NaCl solution at 25 °C.

[c] The number identifies the nominal channel thickness (in µm), i.e. the pillar thickness for the Pillar-profiled membranes, and twice the profile thickness for OCF-profiled membranes.

The OCF-profiled membranes provide to the channel a geometry similar to that of non-woven spacer-filled channels. The OCF profiles were composed of continuous filaments with half-elliptic cross-section with major axis of 1 mm and thickness, representing the semi-minor axis, of either 135 or 75 µm. The distance between two consecutive filaments was 1 mm, with membranes profiled on one side only. CEMs and AEMs were arranged in the stack with their profiles facing each other in the same channel and crossing at 90° (Figure 3a). The thickness of the profile-filled channel was thus twice the profile height (i.e., either 270 or 150 µm). Both OCF-profiled membranes (of either 135 or 75 µm profile thickness) had the same open area, represented by the free (i.e. non-profiled) fraction

of the membrane area, of ~50%. The profile-filled channel had a porosity of ~61%. The main flow was directed at 45° of either filament. Between two adjacent OCF-profiled membranes, a gasket was interposed to seal the lateral regions of the profile-filled channel. It included also a piece of net spacer at the inlet/outlet regions close to the manifolds. Therefore, it confined the solution within the lateral sides of the channel and separated the membranes in the inlet/outlet regions.

The other channel of the cell pair, comprised between the flat sides of two adjacent OCF profiled membranes, was equipped with a woven spacer with integrated gasket. The spacer thickness was equal, or at least similar, with respect to that of the profile-filled channel, namely 270 or 155 μm. The spacers had a pitch-to-height ratio of 2, a porosity of ~75% and an open area of ~50%. Therefore, the stack equipped with OCF-profiled membranes was actually hybrid, having one channel filled by membrane profiles and one channel filled by a net spacer.

The pillar-profiled membranes were characterized by a simpler geometrical configuration. The pillar profiles were semi-ellipsoidal ridges that can be approximated by parallelepipeds with square base with 1 mm side and thickness of 155 μm, placed on one side of the membrane (Figure 3b). The pillar profiles were arranged in a square lattice with $\sqrt{2}$ mm side (distance between the centres). The open area was ~50%, as well as the volume channel porosity. The direction of the main flow was parallel to the diagonal of the profiles and of the lattice. Note that the tested pillar-profiled membranes were characterized by a reduction of active area. In a first approximation, the lateral active area of the pillar, calculated as $1 \times 0.155 \times 4$ mm^2, was ~60% of the area that it subtracted from the adjacent membrane, equal to 1×1 mm^2. Pillar-profiled membranes were arranged in the stack by putting in contact the flat side of each membrane with the profiled side of the adjacent membrane, thus the channel thickness was determined by the profiles height (≈155 μm). Out of the active profiled area, a gasket was placed on each membrane.

For comparison purposes, the experimental campaign of the present study included tests with conventional ED units, using stacks equipped with flat membranes and woven spacers either 270 or 155 µm thick.

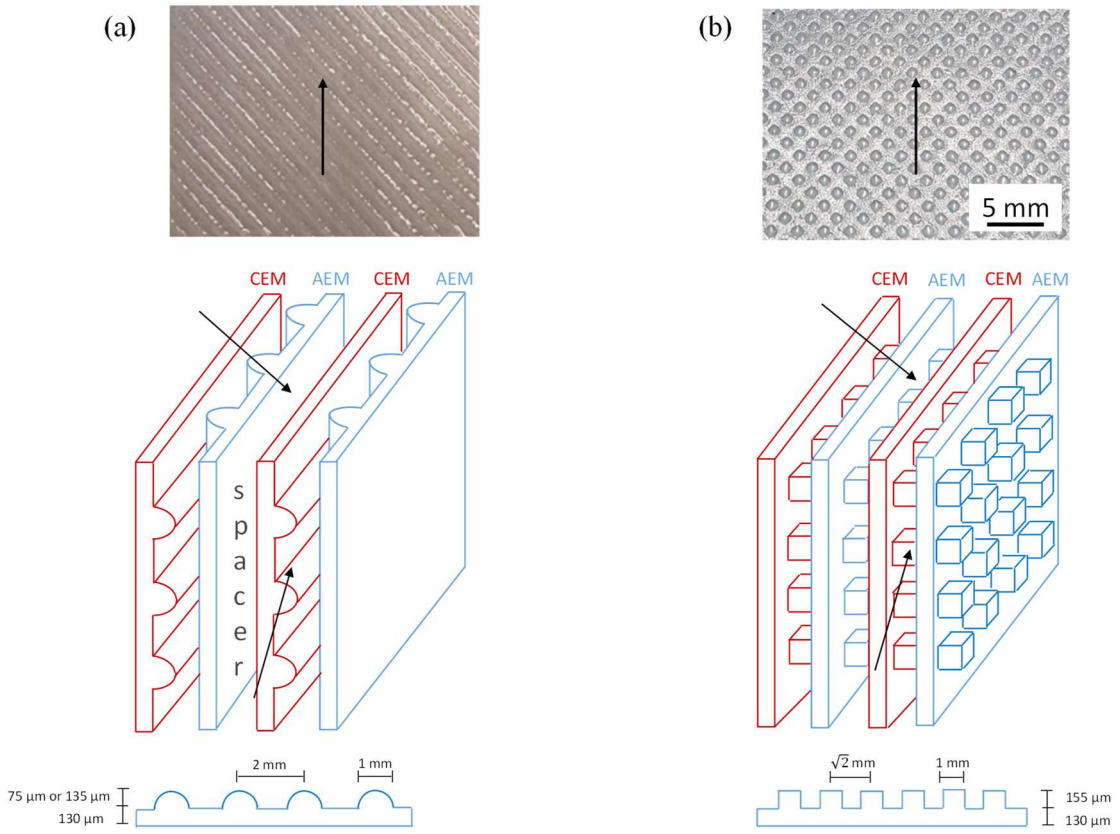

Figure 3. Picture of profiled membranes (top row), schematic representation of the stack assembly (middle row), and schematic cross-section of one profiled membrane (bottom row) with Overlapped Crossed Filament-profiled membranes (a) and Pillar-profiled membranes (b). Arrows indicate the flow direction (cross-flow layout).

The profiled membranes tested in this work are not symmetric, as the profiles were fabricated only on one side of the membrane. Therefore, the two channels of the cell pair were not identical. As a consequence, two different operating mode arisen, regarding the relative direction of the electric current and the position of the two solutions, which could lead to different behaviours and performances. Moreover, stacks with OCF-profiled membranes were in a “hybrid” configuration,

with alternating profile-filled and spacer-filled channels. Therefore, the diluate could flow through the spacer-filled channel with the electric current going from the flat side to the profiled side of the CEM, or *vice versa* (Figure 4). In stacks equipped with pillar-profiled membranes, the compartments were created alternatively by profiles of either the AEM or the CEM. Therefore, the diluate could flow through the channel with AEM pillars, with the electric current going from the flat side to the profiled side of each IEM, or *vice versa* (Figure 5). The two different operating modes for the electric current direction in the stacks will be referred to as "A" and "B" hereafter. They were obtained by switching the current direction (i.e., the electrodes polarity) and, in the case of two inlet streams at different concentration, the diluate and concentrate channels.

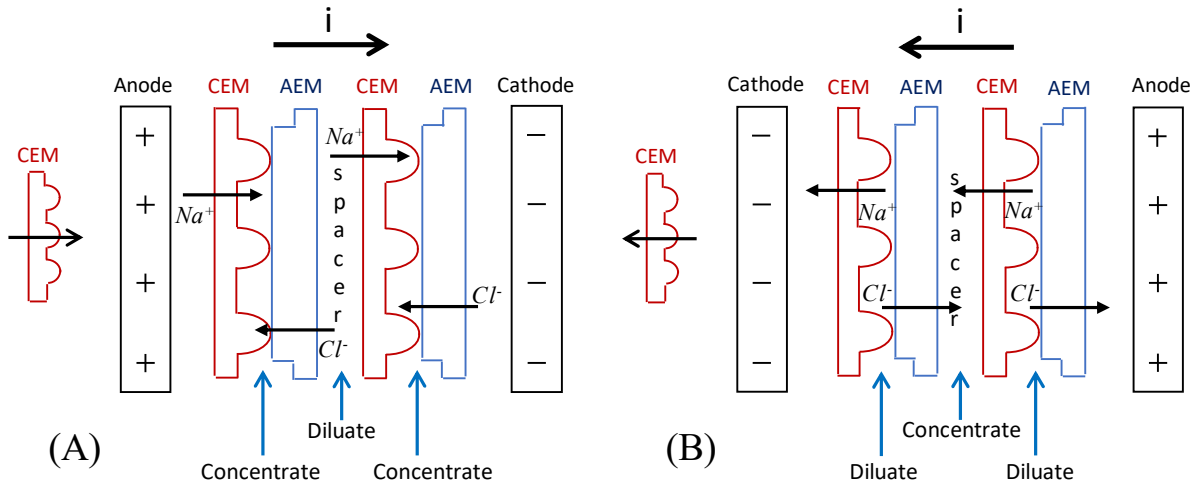

Figure 4. Operating modes for OCF-profiled membrane stack: (A) electric current from flat to profiled side of CEM (i.e., diluate through the spacer-filled channels); (B) electric current from profiled to flat side of the CEM (i.e., diluate through the profile-filled channels).

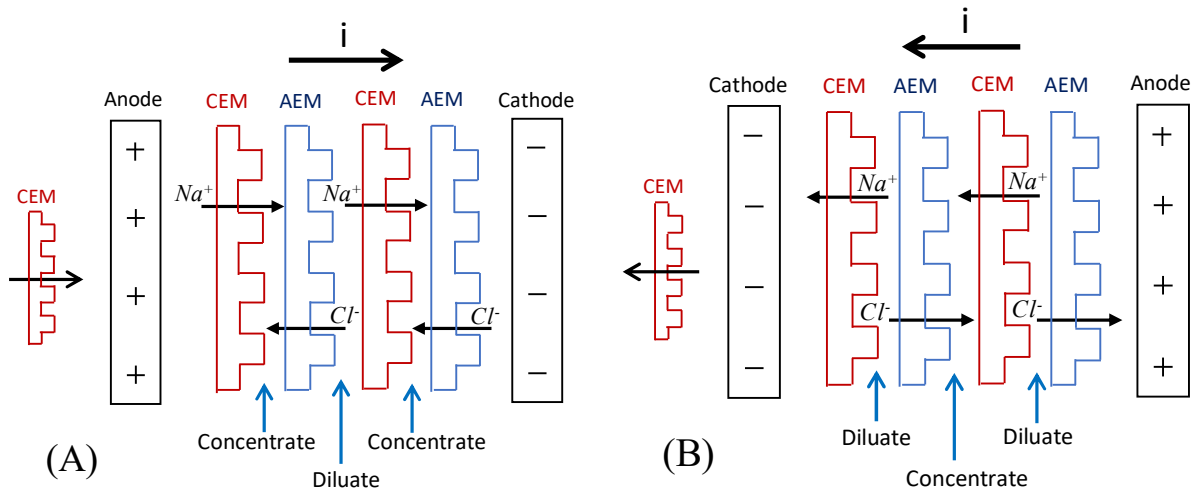

Figure 5. Operating modes for Pillar-profiled membrane stack: (A) electric current from flat to profiled side of each membrane (i.e, diluate through the AEM pillars); (B) electric current from profiled to flat side of each membrane (i.e., diluate through the CEM pillars). For clarity of the graphical representation, the pillar profiles of each membrane are shown detached from the adjacent membrane, though they are actually in contact when piled together within the stack.

Five stacks in total were tested, depending on the membranes used. By taking into account the two operating modes for the electric current in the case of stacks with profiled membranes, the labels indicated in the first and second row of Table 2 will be used hereafter. Table 2 indicates also the diluate and concentrate filling for each case.

Table 2. Labels used to indicate the different stacks (with flat, or OCF-profiled or Pillar-profiled membranes, first row from the top) and the relative direction of the electric current (second row); diluate and concentrate compartment filling for each case (third and fourth row, respectively). The number in the label indicates the thickness of the channel. "A" means that the electric current goes from the flat side to the profiled side of the CEM; "B" means that the electric current goes towards the opposite direction (i.e. from the flat side to the profiled side of the AEM).

Stack	**Flat_270**	**Flat_155**	**OCF_270**		**OCF_150**		**Pillar_155**	
Configuration			**OCF_270_A**	**OCF_270_B**	**OCF_150_A**	**OCF_150_B**	**Pillar_155_A**	**Pillar_155_B**
Diluate	spacer	spacer	spacer	profiles	spacer	profiles	AEM profiles	CEM profiles
Concentrate	spacer	spacer	profiles	spacer	profiles	spacer	CEM profiles	AEM profiles

237 Salt solutions (0.5, 1, 30 or 60 g/l) were prepared with demineralized water and NaCl (>99.5% purity,
238 Saline di Volterra s.r.l., Italy or Regenit, Frisia Zout B.V., The Netherlands), and pumped as single-
239 pass through the stack at different flow rates (see Table 3) with equal values for both streams. NaCl
240 concentrations for concentrate and diluate were chosen to mimic solutions treated in the final stage
241 of a multi-stage ED configuration or of a long stack for seawater desalination [19], as well as for
242 brackish water desalination.

243 Table 3. Operating conditions in terms of fluid velocity and inlet concentration of the salt solutions.

	Concentrate	Diluate
Inlet concentration [g/l NaCl]	0.5	0.5
	30	
	60	
	1	1
	30	
	60	
Fluid velocity [cm/s]	0.25	
	0.5	
	1	

244

245 The stack electrodes consisted of titanium and iridium-MMO (mixed metal oxide) coated electrodes,
246 fixed on a polymethylmethacrylate (PMMA) support. Figure 6 shows the overall experimental setup.
247 The electrode rinse solution (ERS) was an aqueous solution of potassium hexacyanoferrates (II)
248 trihydrate (≥99% purity, Honeywell Fluka™, Germany), potassium hexacyanoferrates (III) (≥99%
249 purity, Honeywell Fluka™, China) and sodium chloride (purity as above) (0.3M $K_3Fe(CN)_6$, 0.3M
250 $K_4Fe(CN)_6 \cdot 3H_2O$, 0.25M NaCl), pumped through the electrode compartments with a flow rate of 180
251 ml/min and recirculated in the ERS reservoir. Peristaltic pumps (Masterflex Cole-Palmer) were used
252 to feed all the solutions. Pulsation dampers were installed at the inlet to minimize pulsation of the
253 peristaltic pumps, ensuring a continuous flow entering the stack.

254 The electric current was supplied to the stack by a potentiostat/galvanostat (Ivium Technologies, The
255 Netherlands). Multimeters (Fluke 175) were used for the electric measurements. The electric

conductivity of the solutions was measured by a portable conductivity-meter (WTW 314i). all experiments were conducted at room temperature (~20 °C).

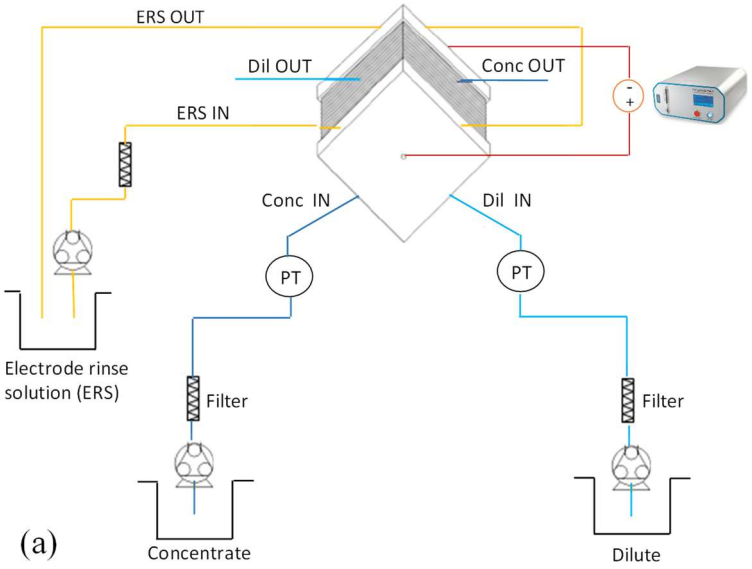

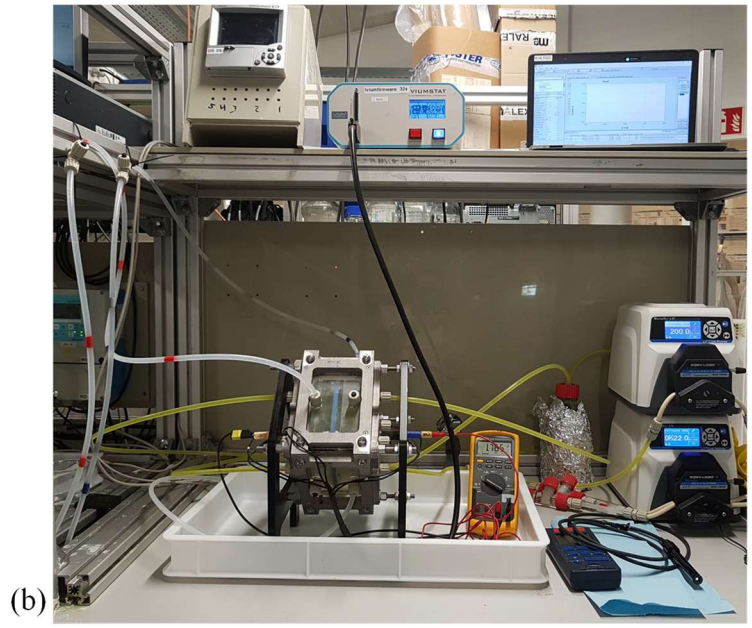

Figure 6. Schematic representation (a) and picture (b) of the experimental set-up.

2.2 Methods

After assembling the stack, hydraulic tests were conducted to detect and fix possible internal and external leakages [66].

Current–voltage characteristics were built from chronopotentiometric measurements. After a short period of open circuit, the current was applied and maintained for about ten times the residence time of the solutions in the stack. The corresponding stationary voltage or its mean value, in the presence of oscillation, was recorded. The applied current was made to increase until it attained the limiting current *plateau* region, in order to collect information both in underlimiting and in limiting conditions. Measurements were taken with two multimeters, one as ammeter and the other as voltmeter, connected in series and in parallel, respectively, to the stack. From the current–voltage curve, the limiting current density (LCD) was identified from the intersection point between the straight line extrapolated from the first linear ohmic tract and the tangent to the second region [67].

The current efficiency represents the fraction of current converted into useful salt flux, which is a measure of how effectively the ion-exchange membranes lead to the selective passage of ions for a given applied current [2]. By using the inlet-outlet mass balance of salt in the diluate channel, the current efficiency (η) was calculated as:

$$\eta = \frac{z\,F\,(Q_{dil,IN}C_{dil,IN} - Q_{dil,OUT}C_{dil,OUT})}{N_{CP}\;I\;M_w} \quad (2)$$

where $Q_{dil,IN}$ and $Q_{dil,OUT}$ are the total diluate flow rates at the inlet and outlet of the stack, respectively, $C_{dil,IN}$ and $C_{dil,OUT}$ are the mass concentrations of salt in the diluate at the inlet and the outlet of the stack, respectively, N_{CP} is the number of cell pairs, I is the electric current, and M_w is the molecular weight of the salt. For each value of applied current, the electrical conductivity was measured for both outlets (diluate and concentrate), and the corresponding NaCl concentrations were calculated by using an empirical correlation [68].

Finally, the specific energy consumption was calculated per unit volume of diluate product (SEC):

$$SEC = \frac{V\,I}{Q_{dil,OUT}} \quad (3)$$

where V is the stack voltage.

3 Results and Discussion

The first part of the experimental campaign was focused on the influence of the operating mode (i.e., current direction, with respect to the membrane profiles), which can have a role in determining the system performance due to the fact that all the investigated profiled membranes are asymmetrical (i.e., single-sided profiled) (section 3.1). Next, the best operating mode (in terms of highest LCD values) was selected for the comparison tests among stacks with profiled membranes against conventional stacks with flat membranes and spacers (section 3.2). In both sections, results are reported for a fluid velocity of 1 cm/s and for two representative inlet concentration pairs, namely $C_{dil,IN} = C_{conc,IN} = 1$ g/l NaCl (brackish water conditions) and $C_{dil,IN} = 0.5$ g/l, $C_{conc,IN} = 60$ g/l NaCl (i.e. mimicking the final stage of a seawater desalination unit). Results at different feed conditions (inlet concentration and fluid velocity) can be found in the Supplementary Data.

3.1 Effect of current direction with respect to the profiles orientation

Figure 7 reports typical results obtained with the OCF_270 profiled membranes, feeding the stack with brackish water ($C_{dil,IN} = C_{conc,IN} = 1$ g/l NaCl), or fresh water/brine-mimicking solutions ($C_{dil,IN} = 0.5$ g/l, $C_{conc,IN} = 60$ g/l NaCl). For both concentration couples, the *i–V* curves (Figure 7a-b) exhibit a different behaviour between the two current directions: after a first tract of overlapping, the two curves depart from each other. The *plateau* region is markedly different, and higher values of current density are reached for case "A" (electric current from the flat side to the OCF-profiled side of the CEM). Therefore, this configuration provided higher values of LCD. This behaviour may be partially explained by the enhanced mixing occurring in the woven spacer-filled channel [62], where the diluate flows (see Figure 4a). However, other reasons need to be claimed, due to the significantly different shape of the *i–V* curves. For example, note that case A and B are fundamentally different because of the different effective CEM (or AEM) area exposed to the diluate. Moreover, the *i–V* curve for the OCF_270_A resembles the typical trend found for homogeneous membranes (as the IEMs

used in this work are), where the curve tends to a saturation (horizontal plateau) due to a gradual attainment of the LCD along the stack [69]. Instead, the OCF_270_B configuration exhibits a lower LCD and a longer inclined plateau, thus resembling the typical trend found for heterogeneous membranes. This behaviour may be due to the presence of OCF profiles inside the diluate, which may act as geometrical heterogeneities (though macroscopic) causing a non-uniform local distribution of current density. In this case, the second region of the *i*–*V* curve can be already associated to an overlimiting state. The higher increase of *i* in the second region compared to the OCF_270_A case (i.e., the lower resistance) is a clue of the fact that other phenomena of ion transport are taking place, namely electroosmotic slip of the second kind (non-equilibrium electroconvection) and water splitting, which are favoured by non-uniform distributions of *i*. By testing similar two-side profiled membranes, a lower resistance in the second region compared to that of flat membranes and spacers was found [3], probably due to the membrane profiles present in the diluate.

The shape of the η–*i* curve (Figure 7c-d) is determined by the non-ideal behaviour of the membranes, and, specifically, by the unwanted transport of co-ions and water (via osmosis/electro-osmosis). All of these fluxes increase with the current density, either because directly affected by the current (i.e., electro-osmosis) or indirectly (salt diffusion and osmosis, which are governed by increasing concentration gradient between concentrate and diluate). Therefore, there are two opposite effects on the current efficiency as the electric current increases: on one side, the higher electro-migration tends to increase η; on the other side, higher undesired fluxes tend to reduce η. The phenomenology is even more complex if we consider that the current density is not uniform, but is higher close to the diluate inlet, where the stack resistance is lower. As the total current increases, the current density tends to increase more in this zone. Therefore, a larger part of the cell pair is subject to a high concentration gradient over the membranes. This behaviour makes co-ion diffusion and osmosis further increase and, in some cases, may explain the reduction of η at high values of electric current. However, this effect cannot be significant when, at the same time, (i) there is a large concentration gradient between

337 the inlet solutions and (ii) the diluate feed is at low concentration, e.g. when 0.5-60 g/l solutions are
338 used. In this case, in fact, the average concentration gradient would increase only negligibly at higher
339 current densities.

340 Therefore, the reduction of η at high values of i must be attributed, at least partially, to other reasons.
341 Some changes in the transport properties of IEMs may occur, leading to a loss of selectivity [70] and
342 to the prevalence of undesired transport mechanisms. As a consequence, the η–i curves exhibited
343 decreasing values after the maximum. These results support the hypothesis of a different response of
344 the profiled IEMs relative to the current direction (or, likewise, to profiles orientation during stack
345 assembly). In particular, higher values of current efficiency were obtained at high values of current
346 density in case A. Under this operating mode, η reached a maximum value over 99% when the
347 concentration gradient between the two solutions was low (1-1 g/l inlet concentrations, Figure 7c),
348 and of ~73% when the concentration gradient between the two solutions was high (0.5-60 g/l inlet
349 concentrations, Figure 7d). Instead, the maximum values of η were of ~98% and ~66% at 1-1 g/l and
350 0.5-60 g/l, respectively, for the worst direction of the electric current (case B).

351 Another possible reason behind (i) the reduction of η after the maximum and (ii) different behaviour
352 of the membranes depending on the electric current direction may be the occurrence of water
353 dissociation. It can be favoured in case B, where "bipolar contacts" (i.e., the contact area between
354 anion-exchange and cation-exchange profiles/membranes) are in the diluate channel and a non-
355 uniform distribution of current may occur. It is known that water splitting depends significantly on
356 the catalytic activity of the functional groups and may occur even in the underlimiting region [71].
357 The ion-exchange matrix of the AEMs used in this work contains mainly quaternary ammonium
358 bases, but also a small amount of secondary and tertiary amines [72], which have a high catalytic
359 activity [71]. Other phenomena reducing the current efficiency could be parasitic currents (or shunt
360 currents) flowing via manifolds. However, given the low number of cell pairs (namely 10), we can
361 reasonably assume that they were negligible in the present experiments [73].

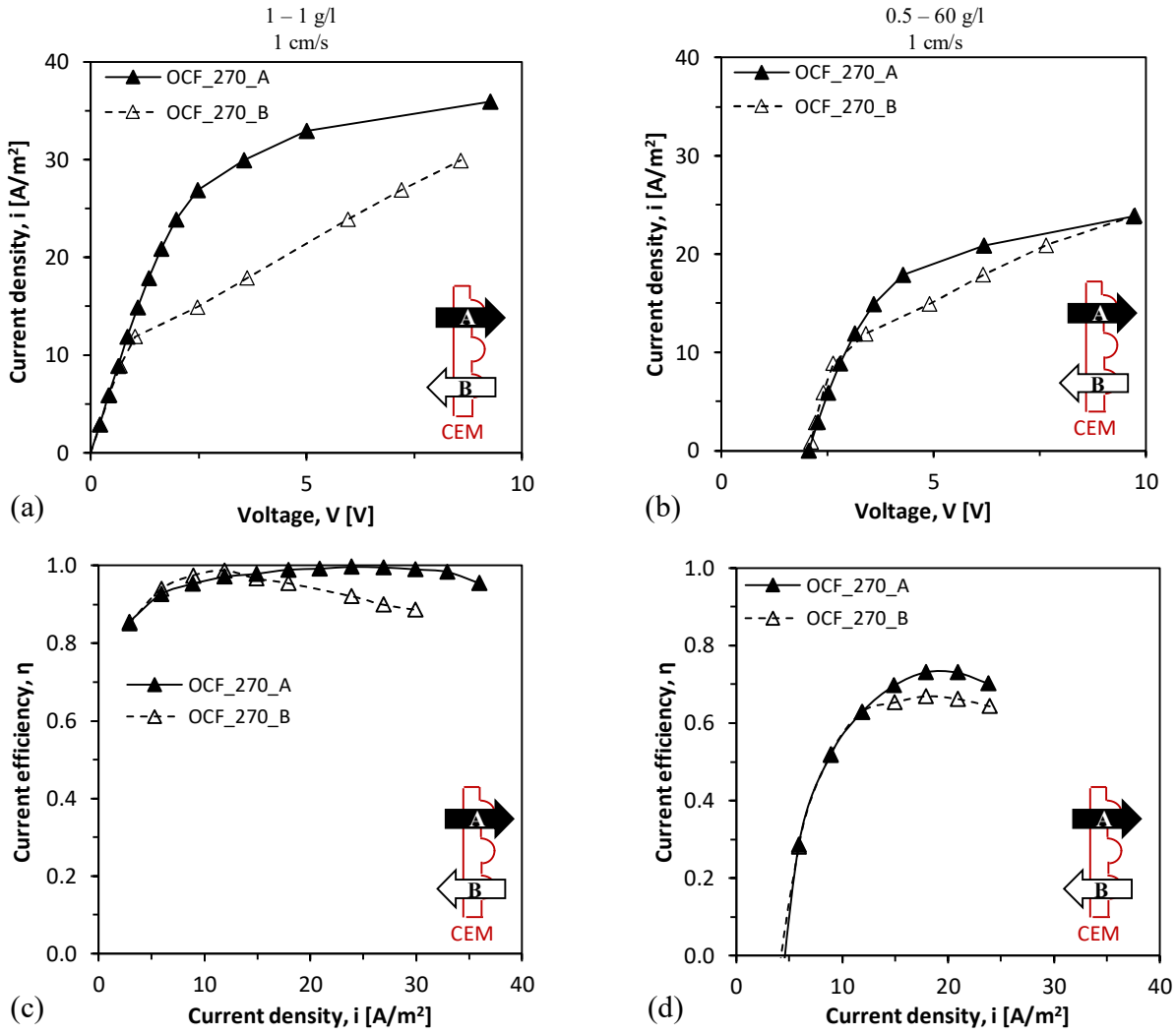

Figure 7. Current density–voltage curves (a,b) and current efficiency–current density curves (c,d) for the OCF_270 stack fed by inlet concentrations of $C_{dil,IN} = C_{conc,IN} = 1$ g/l (a,c) or $C_{dil,IN} = 0.5$ g/l and $C_{conc,IN} = 60$ g/l (b,d) at velocity of 1 cm/s. Two current operating modes are compared: case A (solid symbols) means current from flat side to profiled side of CEM; Case B (hollow symbols) means current from profiled side to flat side of CEM.

In the comparison between the different current directions (case A and B), similar results were obtained in all the investigated operating conditions (in terms of inlet concentrations and velocity). Considering the same stack of Figure 7 (OCF_270), Figure 8a and b show that the LCD increases weakly with the inlet brine concentration and more markedly with the velocity. The trend of the LCD was roughly linear with both variables. In all cases, LCD was significantly higher for the OCF_270_A case (i.e., with profiles in the diluate channel), with the largest relative difference found at equal inlet

concentration (increase of 145% at 1-1 g/l) and decreasing by increasing the brine inlet concentration (increment of 128% at 1-60 g/l) at 1 cm/s. The best current direction enhanced more the LCD at higher velocities, being LCD more than doubled at 1 cm/s with the couple 0.5-60 g/l (Figure 8b). The inlet concentration of the diluate has also an effect on the LCD, as LCD values almost double when increasing the diluate concentration from 0.5 g/l to 1.0 g/l (rightmost points in Figure 8a-b).

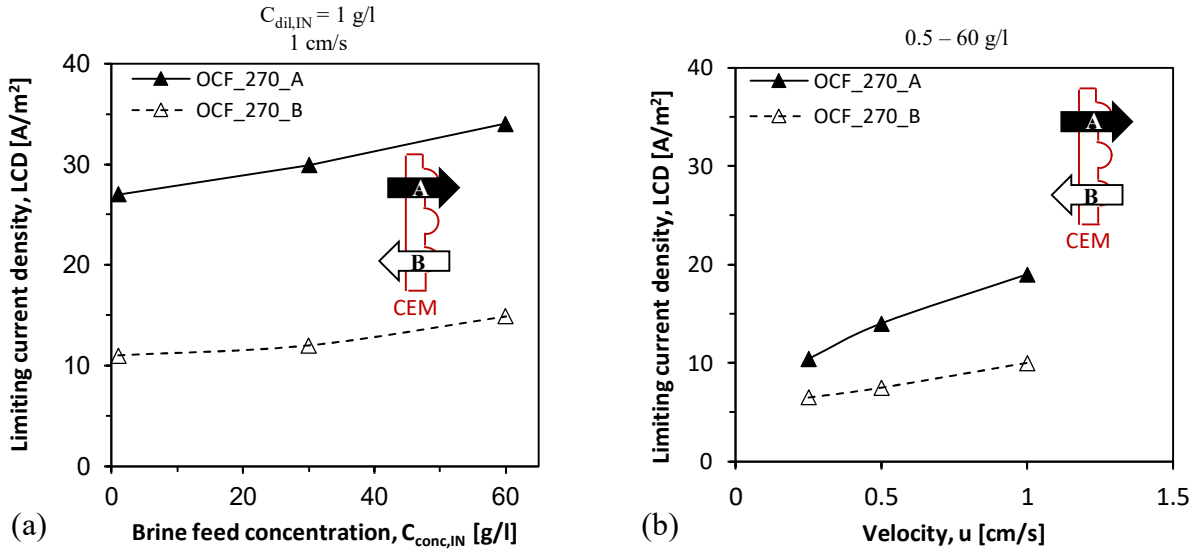

Figure 8. Limiting current density as a function of the concentrate inlet concentration for tests at $C_{dil,IN}$ = 1 g/l and a velocity of 1 cm/s (a) and as a function of the velocity for tests at inlet concentrations of $C_{dil,IN}$ = 0.5 g/l and $C_{conc,IN}$ = 60 g/l (b) for the OCF_270 stack. Two current operating modes are compared: case A (solid symbols) means current from flat side to profiled side of CEM; Case B (hollow symbols) means current from profiled side to flat side of CEM.

Notably, the same behaviour in comparing case A and case B was found when testing the system with other types of profiled membranes (OCF_150 and Pillar_155, see the Supplementary Data). All the investigated profiled membranes showed better performance in the case "A", in terms of higher values of LCD and current efficiency. In the pillar-profiles case, the stack was built only with profiled membranes, since the pillar-shape profile geometry allows for a complete assembly of the stack (i.e., both concentrate and diluate channels), without the need of spacers. As a result, this stack assembly is significantly different from the "hybrid" stack equipped with OCF-profiled membranes (where half

392 of the channels contain spacers). The operating mode with the electric current flowing from the flat
393 side to the pillar-profiled side of each membrane (case A), which exhibited higher LCDs, corresponds
394 to having the diluate in the AEM profile-filled channel. In this case, the diluate compartment faces a
395 larger AEM surface, which likely caused an increase in LCD, for which higher values are normally
396 observed on AEMs than on CEMs [4]. According to Eq. (1), the LCD is theoretically inversely
397 proportional to the difference between the transport numbers of the counter-ion in membrane and
398 solution. While the transport numbers of the counter-ions in the membranes are similar and close to
399 1, the transport numbers in solution are different ($t_{Na^+} \approx 0.4$ and $t_{Cl^-} \approx 0.6$). Therefore, the LCD
400 on the AEM is about 1.5 times higher than that at the CEM [44].

401

402 **3.2 Comparison between profiled and flat membrane stacks**

403 Given the results analysed in section 3.1, the current direction from the flat side to the profiled side
404 of the CEM (case A) was selected for all following experiments, which compares the behaviour of
405 stacks equipped with profiled membranes against stacks equipped with only flat membranes and net
406 spacers.

407 *3.2.1 Current-voltage curve, current efficiency and desalination performance*

408 Figure 9 reports the current density–voltage curves for all stacks tested under different feed conditions
409 (1-1 g/l and 0.5-60 g/l). Although the second couple of concentrations (0.5-60 g/l) implied a higher
410 stack resistance due to the poorly conductive diluate, the two charts are qualitatively similar. All the
411 *i–V* curves exhibit a first linear part, the ohmic region, and a plateau region, with either a gradual
412 reduction of slope towards a horizontal asymptote or an abrupt reduction of slope with an inclined
413 plateau. The first region does not exhibit appreciable differences among all cases, thus indicating that
414 the overall resistance was practically equal for all stacks. Moreover, stacks with similar profiled
415 membranes or spacers (OCF_270_A and OCF_150_A, and flat_270 and flat_155) exhibited the same
416 resistance. This result can be explained by the higher average concentration existing from the diluate

417 when the thickness was higher, due to the lower desalination achieved at a fixed velocity. Therefore,
418 the increase of resistance due to the higher thickness was counterbalanced by the increase of
419 conductivity.
420 All stacks exhibited different limiting current behaviours. The slope in the second region of the *i–V*
421 curve decreased for both the OCF_270_A and the Flat_270 cases. The maximum reduction of slope
422 was reached in the OCF_150_A case, approaching a horizontal plateau. A linear second region was
423 recorded for the Pillar_155_A case, probably because the presence of pillar profiles (of the AEM in
424 case A) within the diluate implies the typical behaviour of systems with locally non-uniform current
425 distribution. Clearly, these results had implications on the LCD. From the intersection point between
426 the straight line extrapolated from the first region and the tangent to the second region [67], it is easy
427 to recognise that the LCD exhibited the following ranking: OCF_270_A > Flat_270 > OCF_150_A
428 > Flat_155 > Pillar_155_A. More details on the LCD are discussed in section 3.2.2.

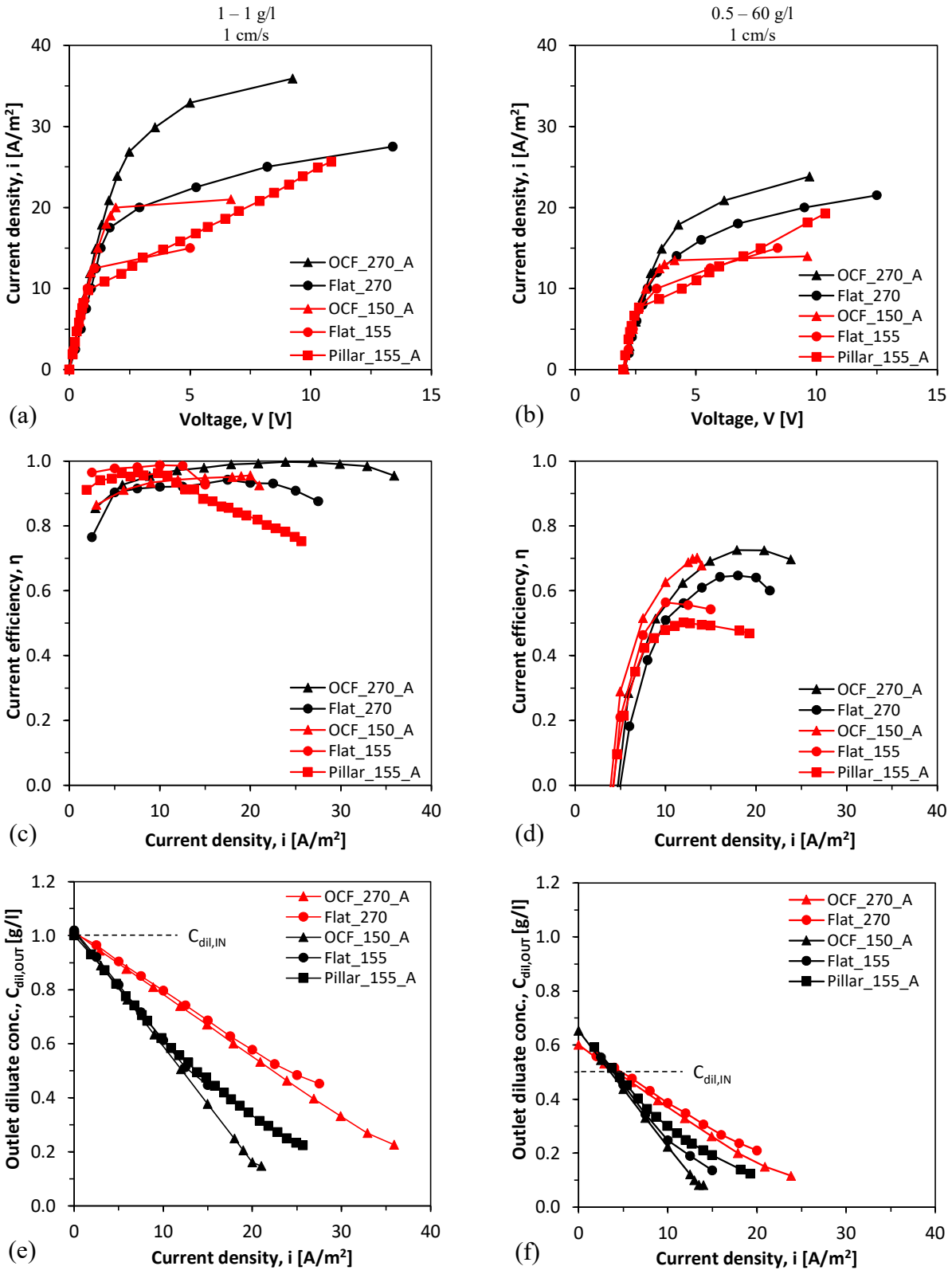

Figure 9. Current density–voltage curves (a,b), current efficiency–current density curves (c,d) and diluate outlet concentration–current density curves (e,f) for all the tested stacks fed by inlet concentrations of $C_{dil,IN}$ = $C_{conc,IN}$ = 1 g/l (a,c,e) or $C_{dil,IN}$ = 0.5 g/l and $C_{conc,IN}$ = 60 g/l (b,d,f) at velocity of 1 cm/s.

Figure 9c and d report the current efficiency as a function of the current density for all stacks tested. The two charts are significantly different. When the concentration gradient between the two compartments was low (1-1 g/l inlet concentrations) η was high (above 85% in most cases) even at low values of i, as expected. Then, it slightly increased, exhibiting maximum values between ~94% and ~99% and, finally, started decreasing roughly over the region of the i–V curve. The OCF_270_A test case provided the highest value of η.

Note that, in the case of large inlet concentration difference, at low current densities the diffusive flux of ions from concentrate to diluate is larger than the electromigrative flux, thus resulting in an concentration at the diluate outlet higher than that at the diluate inlet (Figure 9f), and negative values of current efficiency (Figure 9d) according to the definition of η (Eq. 2). By increasing the current density, the electromigrative flux overcomes the back-diffusive flux of ions, and the current efficiency rapidly increases with the current density (Figure 9d). The value of "critical current density" (i.e., the current leading to a net transport of ions equal to zero and $\eta \approx 0$, [4]) was in the range of 3.5–5 A/m^2. Note that the values of the CCD were practically coincident with those of the current density at which η was zero. In fact, the measured change in flow rate from inlet to outlet was negligible. Given the small entity of (electro-)osmosis compared to salt diffusion, the condition $C_{dil,OUT} = C_{dil,IN}$ corresponded to the condition $\eta = 0$. Then, η increased up to maximum values between ~50% and ~70%, corresponding to the incipient limiting region for all stacks. Finally, η decreased in the rest of the i range tested. By comparing the maximum current efficiency of the stacks, the ranking was similar to that in terms of LCD only for the couple 0.5-60 g/l (OCF_270_A > OCF_150_A > Flat_270 > Flat_155 > Pillar_155_A).

The current efficiency is strictly related to the outlet concentration, which is reported in Figure 9e-f for the diluate. The outlet concentration depends on the mass balance within the cell pair and is affected by unwanted transport phenomena. At 1-1 g/l inlet concentration, the desalination rate was higher than at 0.5-60 g/l due to the higher current efficiency. $C_{dil,OUT}$ followed a linear trend with i in

458 the ohmic region of the *i–V* curve. Then, $C_{dil,OUT}$ reduced at a lower rate when the stack was operated
459 in the limiting/overlimiting region where the current efficiency decreased. By comparing stacks with
460 the same (or at least similar) channel thickness, the OCF_270_A test exhibited a higher desalination
461 rate than the Flat_270 test, thanks to the higher values of η at any i. For the other three cases, the
462 desalination rate was equal only in the under-limiting region at 1-1 g/l. Otherwise, the desalination
463 rates were in descending order reflecting, obviously, that of the current efficiency (OCF_150_A >
464 Flat_155 > Pillar_155_A). Of course, stacks with thicker channels yielded lower desalination rates
465 than stacks with thinner channels, due to the higher flow rate (at fixed velocity).

466 As anticipated above, when the inlet concentrations differ from each other, there exists a non-null
467 value of i that provides zero desalination ($C_{dil,OUT} = C_{dil,IN}$), referred to as "critical current density"
468 (CCD) [4]. The knowledge of this parameter is important to be sure that the achievable LCD is
469 sufficiently higher to guarantee a good flexibility to the unit. In the present experiments at 0.5-60 g/l
470 (Figure 9f), the CCD was below ~5 A/m^2.

471 Results with other couples of inlet concentrations are reported in the Supplementary Data.

472

473 *3.2.2 Influence of operating conditions on limiting current density and energy consumption*

474 Figure 10 summarizes the collected measurements of LCD under different experimental conditions
475 (velocity and inlet concentrations) and for all the different membranes tested. Under the conditions
476 tested, the LCD was approximatively comprised between ~2 and ~35 A/m^2. The LCD had a weak
477 positive dependence on the inlet concentration of the brine (Figure 10 a-b), which can be attributed
478 to the higher concentration at the membrane/solution interface on the diluate side due to the higher
479 back-diffusion. In general, by increasing the diluate concentration from 0.5 g/l to 1.0 g/l, the LCD
480 almost doubled in all the investigated cases, as expected [29–31]. At 1-1 g/l, the LCD was roughly
481 proportional to the fluid velocity, while at 0.5-60 g/l the effect of the velocity was generally lower.

It can be observed that the LCD values recorded were in the following descending order for the various stacks: OCF_270_A > Flat_270 > OCF_150_A > Flat_155 > Pillar_155_A. This confirms what was mentioned in discussing the *i–V* curves in section 3.2.1, but extends that result to various operating conditions. There were only some experimental conditions where exceptions to this ranking occurred. Overall, comparing all the tested cases, the OCF_270_A case (the best one) approximatively tripled the LCD with respect to the Pillar_155_A case (the worst one), while the other configurations had intermediate performances. The stacks with OCF-profiled membranes (OCF_270_A, OCF_150_A) exhibited LCD values ~20% higher than the those with flat membranes (Flat_270, Flat_155), under the same (or very similar) conditions of feed solutions and channel thickness. The presence of the OCF profiles in substitution of the woven spacer in the concentrate compartment led to a different behaviour in the limiting region, which enhanced the LCD (as well as the current efficiency), as seen in section 3.2.1. Instead, the Pillar_155_A case exhibited the worst limiting behaviour and the lowest LCD under all experimental conditions. This configuration was probably affected by a poor mixing in the channel caused by stagnant regions [59,74] and by a reduced active area.

Interestingly, in all the investigated cases the LCD was significantly higher as the channel thickness increases (i.e., OCF_270_A compared to OCF_150_A, and Flat_270 compared to Flat 155, Figure 10). The effect of the channel thickness is not straightforward. According to the classical Nernst theory, LCD is proportional to Sh/*H*, Sh being the Sherwood number and *H* the channel thickness, see Eq. (1). The Sherwood number may increase more or less than linearly with the Reynolds number (and thus with *H*), depending on the channel geometry [62]. Therefore, in general the LCD can either increase or decrease with increasing channel thickness. Note that the woven spacers used in this study are identical from a dimensionless point of view, as they are both characterized by the same pitch-to-height ratio. Instead, the OCF-profile filled channels are not simply scaled, since the profiles have a different shape. Moreover, there could be an indirect effect of the different mass balance on the

different LCD. At the same velocity, stacks with thicker channels have a more concentrated diluate. Further effects can stem from the non-uniform distribution of the current density along the flow direction. From the complex combinations of all these aspects, the effect of *H* on the LCD arises. The increase of the LCD as *H* increases found in the present tests, confirms previous experiments [75].

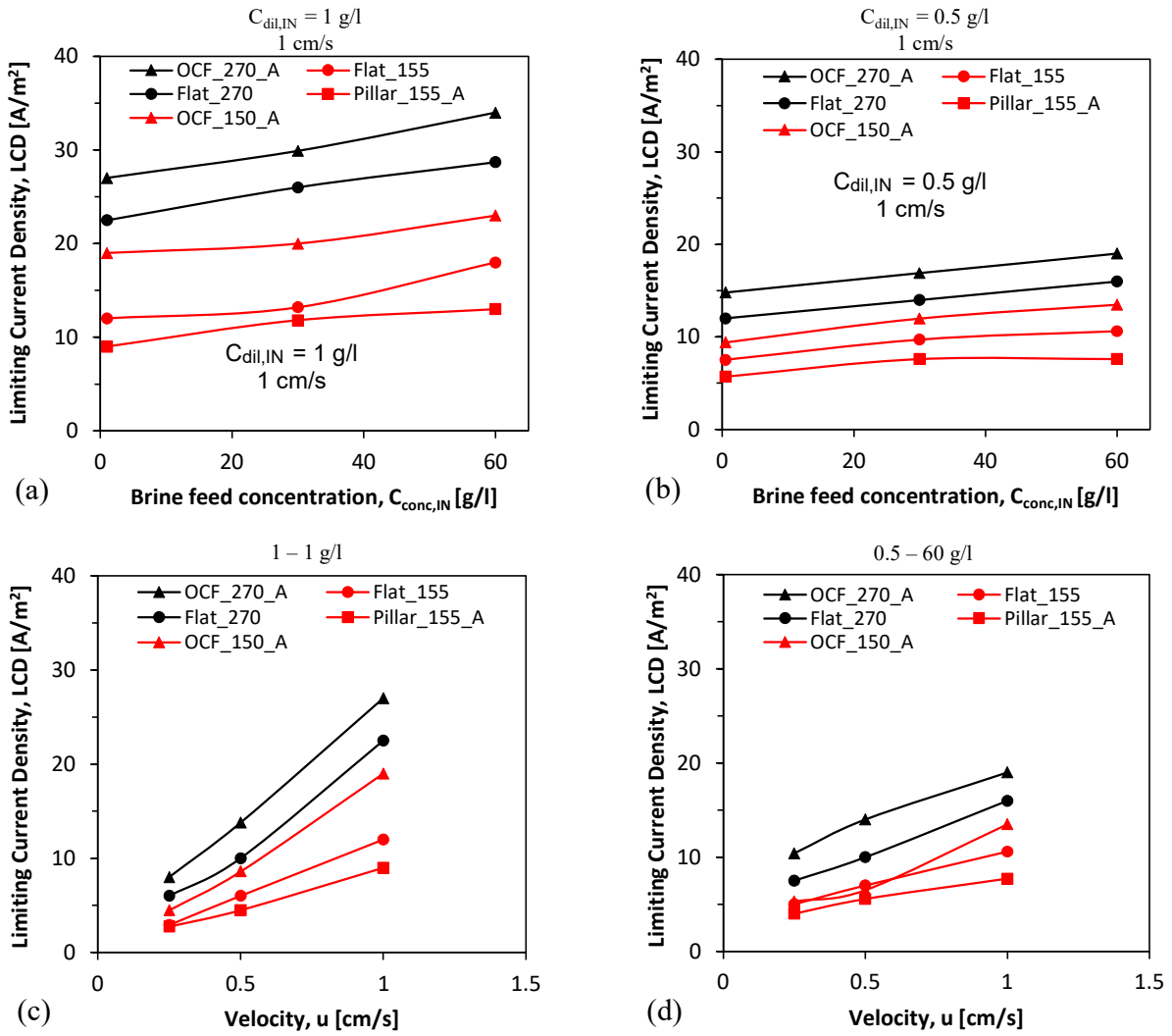

Figure 10. Limiting current density as a function of the concentrate inlet concentration for tests at $C_{dil,IN}$ = 1 g/l (a) or 0.5 g/l (b) at velocity of 1 cm/s; Limiting current density as a function of the velocity for tests at inlet concentrations of $C_{dil,IN}$ = $C_{conc,IN}$ = 1 g/l (c), and $C_{dil,IN}$ = 0.5 g/l and $C_{conc,IN}$ = 60 g/l (d).

In some cases, e.g. Pillar_155_A, the LCD was so low that it was very close to the critical current density. Therefore, higher velocities may be recommended, as they would lead to higher values of the LCD without affecting the CCD. Otherwise, different feed conditions would be needed, if

possible. On the other hand, the OCF_270_A configuration provided LCD values significantly higher than the CCD, thus being more reliable and efficient for reaching the concentration target in the last stages of seawater desalination.

Ohmic resistance, current efficiency and LCD may have a significant impact on the specific energy consumption (SEC) of the different stacks. Figure 11 shows the SEC for the couples of inlet concentrations of 1-1 g/l and 0.5-60 g/l fed at 1 cm/s to desalinate the diluate at an outlet concentration of 0.5 or 0.3 g/l, respectively. By comparing stacks with the same (or very similar) channel thickness, it can be observed that OCF-profiled membranes led to lower SECs than flat membranes, while Pillar-profiled membranes consumed the highest values of energy (OCF_270_A < Flat_270, and OCF_150_A < Flat_155 < Pillar_155_A). In particular, at 1-1 g/l and 0.5-60 g/l the reduction of the SEC was ~78% and ~32% from Flat_270 to OCF_270_A, respectively, while it was ~47% and ~10% from Flat_155 to OCF_150_A, respectively. Instead, the Pillar_155_A configuration increased the SECs roughly by 70% compared to those of the Flat_155 case. The stacks consuming more energy were those requiring a current density falling over the limiting region or, at least, in the last part of the ohmic region (see Figure 9).

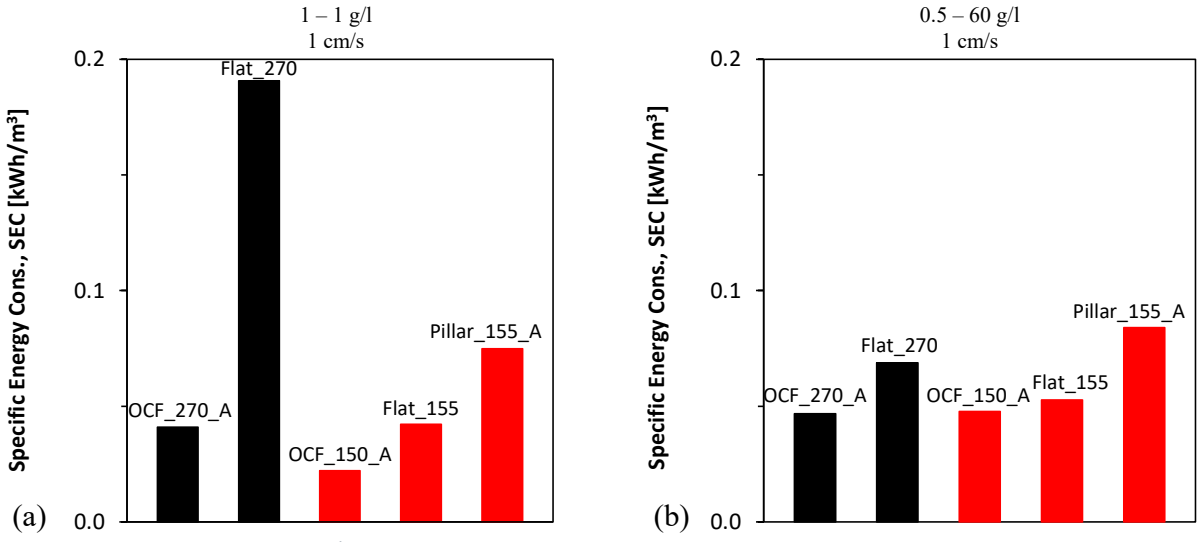

Figure 11. Specific energy consumption for tests at inlet concentrations of $C_{dil,IN}$ = $C_{conc,IN}$ = 1 g/l (a) and $C_{dil,IN}$ = 0.5 g/l and $C_{conc,IN}$ = 60 g/l (b) to obtain a diluate outlet concentration of 0.5 (in graph a) or 0.3 g/l (in graph b), respectively, at velocity of 1 cm/s.

4 Conclusions

The aim of this work has been to investigate the use of asymmetrically profiled membranes in ED for brackish water and seawater desalination, especially focusing on the effect of profile geometry on limiting current density. ED stacks equipped with profiled membranes and conventional (flat) membranes were tested under different operating conditions.

Results showed that the orientation of the electric current with respect to membrane profiles should be carefully taken into account. The operation with the electric current directed from the flat side to the profiled side of the CEM (case "A") was preferable. In stacks with OCF profiled membranes, it corresponds to the configurations with the spacer-filled diluate channels, while, in stacks with pillar profiled membranes, it corresponds to having the diluate channels filled with the AEM pillar profiles. For example, the OCF_270_A case outperformed the alternative case of current direction (OCF_270_B) by exhibiting (i) higher maximum η (e.g. ~73% against ~66% at 0.5-60 g/l inlet concentrations and 1 cm/s) and (ii) roughly double LCDs under various operating conditions. The worse performance in the case OCF_270_B can be explained by the detrimental effects associated to a non-uniform local current distribution caused by the profiles in the diluate. The same current direction led to higher LCDs in the stack equipped with Pillar-profiled membranes (Pillar_155_A case), likely due to the lower difference in the counter-ion transport number between the AEM, which had a higher active area in the diluate, and the diluate itself.

The OCF_270_A and OCF_150_A configurations exhibited better performances than stacks with flat membranes. The maximum η increased, for example, from ~55–65% for Flat_270 and Flat_155 to ~70–73% for OCF_270_A and OCF_150_A at 0.5-60 g/l inlet concentrations. The LCD increased roughly by 20% under various operating conditions. Instead, the stack with Pillar-profiled membranes, even when operated with the best current direction (Pillar_155_A case), yielded worse performances compared to the Flat_155 stack, probably due to the detrimental effects associated to a locally non-uniform current distribution in the diluate and to a poor mixing. Under most operating

conditions, the measured LCD values were in the following descending order: OCF_270_A > Flat_270 > OCF_150_A > Flat_155 > Pillar_155_A. The OCF_270_A configuration gave LCDs approximatively tripled with respect to the Pillar_155_A configuration, while the other stacks exhibited intermediate performances. Stacks with only woven spacers (e.g. Flat_270) achieved performances somehow in between those of the hybrid stacks with OCF profiles and woven spacers with one or the other direction of the electric current (e.g. OCF_270_A and OCF_270_B).

The specific energy consumption calculated for a diluate desalination of 0.5 g/l or 0.2 g/l for 1-1 g/l or 0.5-60 g/l inlet concentrations, respectively, was reduced by OCF-profiled membranes by 10–78%. This resulted from the fact that stacks with flat membranes required overlimiting currents. By resulting in higher η and LCD, profiled membranes may reduce membrane area and capital costs. Moreover, well-designed profiled membranes can reduce the overall desalination cost, thus prompting the development of competitive systems in applications where ED has been too much expensive so far. In particular, OCF-profiled membranes are very promising and deserve further studies.

Symmetrical (i.e. double-sided) profiled membranes would be of interest to ensure good performance also during polarity switch for fouling removal in EDR operations. However, fabricating double-sided profiled membranes with homogeneous and regular profile structure is still technically challenging, and further research efforts are needed in this regard. Moreover, the profile geometry should be optimized to ensure better performances compared to those achieved with conventional stacks with flat membranes and net spacers.

Acknowledgments

This work was performed in the framework of the REvivED water project (Low energy solutions for drinking water production by a REvival of ElectroDialysis systems). This project has received

586 funding from the European Union's Horizon 2020 Research and Innovation program under Grant
587 Agreement no. 685579 (www.revivedwater.eu).

588 The authors are also grateful to REDstack B.V. for supplying the ED stack and to Fujifilm
589 Manufacturing Europe B.V. for supplying all the membranes for this study.

590

591 **List of abbreviations**

592 AEM Anion-exchange membrane

593 CCD Critical current density

594 CEM Cation-exchange membrane

595 ED Electrodialysis

596 IEM Ion-exchange membrane

597 LCD Limiting current density

598 OCF Overlapped crossed filament

599 SEC Specific energy consumption

600

601 **References**

602 [1] A. Campione, L. Gurreri, M. Ciofalo, G. Micale, A. Tamburini, A. Cipollina, Electrodialysis
603 for water desalination: A critical assessment of recent developments on process fundamentals,
604 models and applications, Desalination. 434 (2018) 121–160. doi:10.1016/j.desal.2017.12.044.

605 [2] J.R. Wilson, Demineralization by electrodialysis, Butterworths Scientific Publications,
606 London, 1960.

607 [3] H. Strathmann, Electrodialysis, a mature technology with a multitude of new applications,

608 Desalination. 264 (2010) 268–288. doi:10.1016/j.desal.2010.04.069.

609 [4] M. La Cerva, L. Gurreri, M. Tedesco, A. Cipollina, M. Ciofalo, A. Tamburini, G. Micale,
610 Determination of limiting current density and current efficiency in electrodialysis units,
611 Desalination. 445 (2018) 138–148. doi:10.1016/j.desal.2018.07.028.

612 [5] C. Huang, T. Xu, Y. Zhang, Y. Xue, G. Chen, Application of electrodialysis to the production
613 of organic acids: State-of-the-art and recent developments, J. Memb. Sci. 288 (2007) 1–12.
614 doi:10.1016/j.memsci.2006.11.026.

615 [6] T. Xu, C. Huang, Electrodialysis-Based separation technologies: A critical review, AIChE J.
616 54 (2008) 3147–3159. doi:10.1002/aic.11643.

617 [7] J. Ran, L. Wu, Y. He, Z. Yang, Y. Wang, C. Jiang, L. Ge, E. Bakangura, T. Xu, Ion exchange
618 membranes: New developments and applications, J. Memb. Sci. 522 (2017) 267–291.
619 doi:10.1016/j.memsci.2016.09.033.

620 [8] L. Gurreri, A. Tamburini, A. Cipollina, G. Micale, Electrodialysis applications in wastewater
621 treatments for environmental protection and resources recovery: a systematic review on
622 progress and perspectives, Membranes (Basel). 10 (2020) 1–82.
623 doi:10.3390/membranes10070146.

624 [9] International Desalination Association (IDA), Desalination Yearbook 2016-2017, 2017.

625 [10] E. Jones, M. Qadir, M.T.H. van Vliet, V. Smakhtin, S. mu Kang, The state of desalination and
626 brine production: A global outlook, Sci. Total Environ. 657 (2019) 1343–1356.
627 doi:10.1016/j.scitotenv.2018.12.076.

628 [11] A. Al-Karaghouli, L.L. Kazmerski, Energy consumption and water production cost of
629 conventional and renewable-energy-powered desalination processes, Renew. Sustain. Energy
630 Rev. 24 (2013) 343–356. doi:10.1016/j.rser.2012.12.064.

631 [12] REvivED water, https://www.revivedwater.eu/.

[13] R.K. McGovern, S.M. Zubair, J.H. Lienhard V, The cost effectiveness of electrodialysis for diverse salinity applications, Desalination. 348 (2014) 57–65. doi:10.1016/j.desal.2014.06.010.

[14] K.M. Chehayeb, K.G. Nayar, J.H. Lienhard, On the merits of using multi-stage and counterflow electrodialysis for reduced energy consumption, Desalination. 439 (2018) 1–16. doi:10.1016/j.desal.2018.03.026.

[15] M. La Cerva, L. Gurreri, A. Cipollina, A. Tamburini, M. Ciofalo, G. Micale, Modelling and cost analysis of hybrid systems for seawater desalination: Electromembrane pre-treatments for Reverse Osmosis, Desalination. 467 (2019) 175–195. doi:10.1016/j.desal.2019.06.010.

[16] A. Campione, A. Cipollina, I.D.L. Bogle, L. Gurreri, A. Tamburini, M. Tedesco, G. Micale, A hierarchical model for novel schemes of electrodialysis desalination, Desalination. 465 (2019) 79–93. doi:10.1016/J.DESAL.2019.04.020.

[17] M.M. Generous, N.A.A. Qasem, S.M. Zubair, The significance of modeling electrodialysis desalination using multi-component saline water, Desalination. (2020) 114347. doi:10.1016/j.desal.2020.114347.

[18] A.H. Galama, M. Saakes, H. Bruning, H.H.M. Rijnaarts, J.W. Post, Seawater predesalination with electrodialysis, Desalination. 342 (2014) 61–69. doi:10.1016/j.desal.2013.07.012.

[19] G.J. Doornbusch, M. Tedesco, J.W. Post, Z. Borneman, K. Nijmeijer, Experimental investigation of multistage electrodialysis for seawater desalination, Desalination. 464 (2019) 105–114. doi:10.1016/j.desal.2019.04.025.

[20] G.J. Doornbusch, M. Bel, M. Tedesco, J.W. Post, Z. Borneman, K. Nijmeijer, Effect of membrane area and membrane properties in multistage electrodialysis on seawater desalination performance, J. Memb. Sci. 611 (2020) 118303. doi:10.1016/j.memsci.2020.118303.

[21] S. Porada, W.J. van Egmond, J.W. Post, M. Saakes, H.V.M. Hamelers, Tailoring ion exchange

membranes to enable low osmotic water transport and energy efficient electrodialysis, J. Memb. Sci. 552 (2018) 22–30. doi:10.1016/j.memsci.2018.01.050.

[22] J. Kamcev, C.M. Doherty, K.P. Lopez, A.J. Hill, D.R. Paul, B.D. Freeman, Effect of fixed charge group concentration on salt permeability and diffusion coefficients in ion exchange membranes, J. Memb. Sci. 566 (2018) 307–316. doi:10.1016/j.memsci.2018.08.053.

[23] J. Kamcev, D.R. Paul, G.S. Manning, B.D. Freeman, Ion Diffusion Coefficients in Ion Exchange Membranes: Significance of Counterion Condensation, Macromolecules. 51 (2018) 5519–5529. doi:10.1021/acs.macromol.8b00645.

[24] M. Ciofalo, M. Di Liberto, L. Gurreri, M. La Cerva, L. Scelsi, G. Micale, Mass transfer in ducts with transpiring walls, Int. J. Heat Mass Transf. 132 (2019) 1074–1086. doi:10.1016/J.IJHEATMASSTRANSFER.2018.12.059.

[25] D. Butylskii, I. Moroz, K. Tsygurina, S. Mareev, Effect of Surface Inhomogeneity of Ion-Exchange Membranes on the Mass Transfer Efficiency in Pulsed Electric Field Modes, Membranes (Basel). 10 (2020) 40. doi:10.3390/membranes10030040.

[26] F. Sheng, N.U. Afsar, Y. Zhu, L. Ge, T. Xu, PVA-based mixed matrix membranes comprising ZSM-5 for cations separation, Membranes (Basel). 10 (2020) 1–16. doi:10.3390/membranes10060114.

[27] W.J. Koros, Y.H. Ma, T. Shimidzu, Terminology for membranes and membrane processes (IUPAC Recommendations 1996), Pure Appl. Chem. 68 (1996) 1479–1489. doi:10.1351/pac199668071479.

[28] V. V. Nikonenko, N.D. Pismenskaya, E.I. Belova, P. Sistat, P. Huguet, G. Pourcelly, C. Larchet, Intensive current transfer in membrane systems: Modelling, mechanisms and application in electrodialysis, Adv. Colloid Interface Sci. 160 (2010) 101–123. doi:10.1016/j.cis.2010.08.001.

[29] T.L. Hill, G. Scatchard, B.A. Pethica, I.J. Straub, R. Schlögl, G. Manecke, R. Schlögl, M. Nagasawa, I. Kagawa, P. Meares, K. Sollner, F.L. Tye, A. Despiá, G.J. Hills, F. Helfferich, J.E. Salmon, R.J.P. Williams, A.M. Peers, F. Bergsma, A.J. Staverman, N. Krishnaswamy, F. Runge, F. Wolf, E. Glueckauf, D. Reichenberg, R. Neihof, R.D. Keynes, A.R. Ubbelohde, R.M. Barrer, General discussion, Discuss. Faraday Soc. 21 (1956) 117–140. doi:10.1039/DF9562100117.

[30] F. Helfferich, Ion exchange, McGraw-Hill, New York, 1962.

[31] V.G. Levich, Physicochemical Hydrodynamics, Prentice-Hall, Englewood Cliffs, N.J., 1962.

[32] V. V. Nikonenko, S.A. Mareev, N.D. Pis'menskaya, A.M. Uzdenova, A. V. Kovalenko, M.K. Urtenov, G. Pourcelly, Effect of electroconvection and its use in intensifying the mass transfer in electrodialysis (Review), Russ. J. Electrochem. 53 (2017) 1122–1144. doi:10.1134/S1023193517090099.

[33] H.J. Lee, H. Strathmann, S.H. Moon, Determination of the limiting current density in electrodialysis desalination as an empirical function of linear velocity, Desalination. 190 (2006) 43–50. doi:10.1016/j.desal.2005.08.004.

[34] Y. Sano, X. Bai, S. Amagai, A. Nakayama, Effect of a porous spacer on the limiting current density in an electro-dialysis desalination, Desalination. 444 (2018) 151–161. doi:10.1016/j.desal.2018.01.034.

[35] N.C. Wright, S.R. Shah, S.E. Amrose, A.G. Winter, A robust model of brackish water electrodialysis desalination with experimental comparison at different size scales, Desalination. 443 (2018) 27–43. doi:10.1016/j.desal.2018.04.018.

[36] C.C.N. Kunrath, D.C. Patrocínio, M.A. Siqueira Rodrigues, T. Benvenuti, F.D.R. Amado, Electrodialysis reversal as an alternative treatment for producing drinking water from brackish river water: A case study in the dry season, northeastern Brazil, J. Environ. Chem. Eng. 8

(2020) 103719. doi:10.1016/j.jece.2020.103719.

[37] R. Simons, Water splitting in ion exchange membranes, Electrochim. Acta. 30 (1985) 275–282. doi:10.1016/0013-4686(85)80184-5.

[38] V. Nikonenko, M. Urtenov, S. Mareev, G. Pourcelly, Mathematical modeling of the effect of water splitting on ion transfer in the depleted diffusion layer near an ion-exchange membrane, Membranes (Basel). 10 (2020). doi:10.3390/membranes10020022.

[39] V. V. Nikonenko, A. V. Kovalenko, M.K. Urtenov, N.D. Pismenskaya, J. Han, P. Sistat, G. Pourcelly, Desalination at overlimiting currents: State-of-the-art and perspectives, Desalination. 342 (2014) 85–106. doi:10.1016/j.desal.2014.01.008.

[40] A. Uzdenova, M. Urtenov, Potentiodynamic and galvanodynamic regimes of mass transfer in flow-through electrodialysis membrane systems: Numerical simulation of electroconvection and current-voltage curve, Membranes (Basel). 10 (2020). doi:10.3390/membranes10030049.

[41] V.I. Zabolotsky, V. V. Nikonenko, N.D. Pismenskaya, E. V. Laktionov, M.K. Urtenov, H. Strathmann, M. Wessling, G.H. Koops, Coupled transport phenomena in overlimiting current electrodialysis, Sep. Purif. Technol. 14 (1998) 255–267. doi:10.1016/S1383-5866(98)00080-X.

[42] J.J. Krol, M. Wessling, H. Strathmann, Chronopotentiometry and overlimiting ion transport through monopolar ion exchange membranes, J. Memb. Sci. 162 (1999) 155–164. doi:10.1016/S0376-7388(99)00134-9.

[43] B. Zaltzman, I. Rubinstein, Electro-osmotic slip and electroconvective instability, J. Fluid Mech. 579 (2007) 173–226. doi:10.1017/S0022112007004880.

[44] R. Kwak, G. Guan, W.K. Peng, J. Han, Microscale electrodialysis: Concentration profiling and vortex visualization, Desalination. 308 (2013) 138–146. doi:10.1016/j.desal.2012.07.017.

[45] I. Rubinstein, Electroconvection at an electrically inhomogeneous permselective interface,

728 Phys. Fluids A. 3 (1991) 2301–2309. doi:10.1063/1.857869.

729 [46] J. Balster, M.H. Yildirim, D.F. Stamatialis, R. Ibanez, R.G.H. Lammertink, V. Jordan, M.
730 Wessling, Morphology and microtopology of cation-exchange polymers and the origin of the
731 overlimiting current, J. Phys. Chem. B. 111 (2007) 2152–2165. doi:10.1021/jp068474t.

732 [47] V. Nikonenko, A. Nebavsky, S. Mareev, A. Kovalenko, M. Urtenov, G. Pourcelly, Modelling
733 of Ion Transport in Electromembrane Systems: Impacts of Membrane Bulk and Surface
734 Heterogeneity, Appl. Sci. 9 (2018) 25. doi:10.3390/app9010025.

735 [48] V. V. Gil, M.A. Andreeva, L. Jansezian, J. Han, N.D. Pismenskaya, V. V. Nikonenko, C.
736 Larchet, L. Dammak, Impact of heterogeneous cation-exchange membrane surface
737 modification on chronopotentiometric and current–voltage characteristics in NaCl, CaCl2 and
738 MgCl2 solutions, Electrochim. Acta. 281 (2018) 472–485.
739 doi:10.1016/j.electacta.2018.05.195.

740 [49] S. Zyryanova, S. Mareev, V. Gil, E. Korzhova, N. Pismenskaya, V. Sarapulova, O. Rybalkina,
741 E. Boyko, C. Larchet, L. Dammak, V. Nikonenko, How electrical heterogeneity parameters of
742 ion-exchange membrane surface affect the mass transfer and water splitting rate in
743 electrodialysis, Int. J. Mol. Sci. 21 (2020) 973. doi:10.3390/ijms21030973.

744 [50] K.A. Nebavskaya, V. V. Sarapulova, K.G. Sabbatovskiy, V.D. Sobolev, N.D. Pismenskaya, P.
745 Sistat, M. Cretin, V. V. Nikonenko, Impact of ion exchange membrane surface charge and
746 hydrophobicity on electroconvection at underlimiting and overlimiting currents, J. Memb. Sci.
747 523 (2017) 36–44. doi:10.1016/j.memsci.2016.09.038.

748 [51] V. Titorova, K. Sabbatovskiy, V. Sarapulova, E. Kirichenko, V. Sobolev, K. Kirichenko,
749 Characterization of MK-40 membrane modified by layers of cation exchange and anion
750 exchange polyelectrolytes, Membranes (Basel). 10 (2020) 20.
751 doi:10.3390/membranes10020020.

752 [52] C. Larchet, V.I. Zabolotsky, N. Pismenskaya, V. V. Nikonenko, A. Tskhay, K. Tastanov, G.
753 Pourcelly, Comparison of different ED stack conceptions when applied for drinking water
754 production from brackish waters, Desalination. 222 (2008) 489–496.
755 doi:10.1016/j.desal.2007.02.067.

756 [53] S. Pawlowski, J.G. Crespo, S. Velizarov, Profiled ion exchange membranes: A comprehensible
757 review, Int. J. Mol. Sci. 20 (2019) 165. doi:10.3390/ijms20010165.

758 [54] D.A. Vermaas, D. Kunteng, M. Saakes, K. Nijmeijer, Fouling in reverse electrodialysis under
759 natural conditions, Water Res. 47 (2013) 1289–1298. doi:10.1016/j.watres.2012.11.053.

760 [55] J. Balster, D.F. Stamatialis, M. Wessling, Membrane with integrated spacer, J. Memb. Sci. 360
761 (2010) 185–189. doi:10.1016/j.memsci.2010.05.011.

762 [56] Y. Zhao, H. Wang, C. Jiang, L. Wu, T. Xu, Electrodialysis with notched ion exchange
763 membranes: Experimental investigations and computational fluid dynamics simulations, Sep.
764 Purif. Technol. 130 (2014) 102–111. doi:10.1016/j.seppur.2014.04.010.

765 [57] S. Melnikov, S. Loza, M. Sharafan, V. Zabolotskiy, Electrodialysis treatment of secondary
766 steam condensate obtained during production of ammonium nitrate. Technical and economic
767 analysis, Sep. Purif. Technol. 157 (2016) 179–191. doi:10.1016/j.seppur.2015.11.025.

768 [58] D.A. Vermaas, M. Saakes, K. Nijmeijer, Power generation using profiled membranes in
769 reverse electrodialysis, J. Memb. Sci. 385–386 (2011) 234–242.
770 doi:10.1016/j.memsci.2011.09.043.

771 [59] L. Gurreri, M. Ciofalo, A. Cipollina, A. Tamburini, W. Van Baak, G. Micale, CFD modelling
772 of profiled-membrane channels for reverse electrodialysis, Desalin. Water Treat. 55 (2015)
773 3404–3423. doi:10.1080/19443994.2014.940651.

774 [60] J.G.D. Tadimeti, V. Kurian, A. Chandra, S. Chattopadhyay, Corrugated membrane surfaces
775 for effective ion transport in electrodialysis, J. Memb. Sci. 499 (2016) 418–428.

776 doi:10.1016/j.memsci.2015.11.001.

777 [61] L. Gurreri, G. Battaglia, A. Tamburini, A. Cipollina, G. Micale, M. Ciofalo, Multi-physical
778 modelling of reverse electrodialysis, Desalination. 423 (2017) 52–64.
779 doi:10.1016/j.desal.2017.09.006.

780 [62] M. La Cerva, M. Di Liberto, L. Gurreri, A. Tamburini, A. Cipollina, G. Micale, M. Ciofalo,
781 Coupling CFD with a one-dimensional model to predict the performance of reverse
782 electrodialysis stacks, J. Memb. Sci. 541 (2017) 595–610. doi:10.1016/j.memsci.2017.07.030.

783 [63] G. Battaglia, L. Gurreri, G. Airò Farulla, A. Cipollina, A. Pirrotta, G. Micale, M. Ciofalo,
784 Membrane Deformation and Its Effects on Flow and Mass Transfer in the Electromembrane
785 Processes, Int. J. Mol. Sci. 20 (2019) 1840. doi:10.3390/IJMS20081840.

786 [64] G. Battaglia, L. Gurreri, A. Cipollina, A. Pirrotta, S. Velizarov, M. Ciofalo, G. Micale, Fluid–
787 Structure Interaction and Flow Redistribution in Membrane-Bounded Channels, Energies. 12
788 (2019) 4259. doi:10.3390/EN12224259.

789 [65] G. Battaglia, L. Gurreri, G.A. Farulla, A. Cipollina, A. Pirrotta, G. Micale, M. Ciofalo,
790 Pressure-induced deformation of pillar-type profiled membranes and its effects on flow and
791 mass transfer, Computation. 7 (2019) 1–14. doi:10.3390/computation7020032.

792 [66] E. V. Laktionov, N.D. Pismenskaya, V. V. Nikonenko, V.I. Zabolotsky, Method of
793 electrodialysis stack testing with the feed solution concentration regulation, Desalination. 151
794 (2003) 101–116. doi:10.1016/S0011-9164(02)00988-8.

795 [67] M.S. Isaacson, A.A. Sonin, Sherwood Number and Friction Factor Correlations for
796 Electrodialysis Systems, with Application to Process Optimization, 1976.
797 doi:10.1021/i260058a017.

798 [68] S.S. Islam, R.L. Gupta, K. Ismail, Extension of the Falkenhagen-Leist–Kelbg Equation to the
799 Electrical Conductance of Concentrated Aqueous Electrolytes, J. Chem. Eng. Data. 36 (1991)

800 102–104. doi:10.1021/je00001a031.

801 [69] E. Volodina, N. Pismenskaya, V. Nikonenko, C. Larchet, G. Pourcelly, 5on-exchange
802 membranes with homogeneous and heterogeneous surfaces, J. Colloid Interface Sci. 285
803 (2005) 247–258. doi:10.1016/j.jcis.2004.11.017.

804 [70] M.B. Kristensen, A. Bentien, M. Tedesco, J. Catalano, Counter-ion transport number and
805 membrane potential in working membrane systems, J. Colloid Interface Sci. 504 (2017) 800–
806 813. doi:10.1016/j.jcis.2017.06.010.

807 [71] N.D. Pismenskaya, E.D. Melnikova, O.A. Rybalkina, V. V. Nikonenko, The Impact of Long-
808 Time Operation of an Anion-Exchange Membrane AMX-Sb in the Electrodialysis
809 Desalination of Sodium Chloride Solution on the Membrane Current–Voltage Characteristic
810 and the Water Splitting Rate, Membr. Membr. Technol. 1 (2019) 88–98.
811 doi:10.1134/s2517751619020070.

812 [72] Sarapulova, Shkorkina, Mareev, Pismenskaya, Kononenko, Larchet, Dammak, Nikonenko,
813 Transport Characteristics of Fujifilm Ion-Exchange Membranes as Compared to
814 Homogeneous Membranes AMX and CMX and to Heterogeneous Membranes MK-40 and
815 MA-41, Membranes (Basel). 9 (2019) 84. doi:10.3390/membranes9070084.

816 [73] A. Culcasi, L. Gurreri, A. Zaffora, A. Cosenza, A. Tamburini, A. Cipollina, G. Micale, Ionic
817 shortcut currents via manifolds in reverse electrodialysis stacks, Desalination. 485 (2020)
818 114450. doi:10.1016/j.desal.2020.114450.

819 [74] F. Dong, D. Jin, S. Xu, L. Xu, X. Wu, P. Wang, Q. Leng, R. Xi, Numerical simulation of flow
820 and mass transfer in profiled membrane channels for reverse electrodialysis, Chem. Eng. Res.
821 Des. 157 (2020) 77–91. doi:10.1016/j.cherd.2020.02.025.

822 [75] X.W. Zhong, W.R. Zhang, Z.Y. Hu, H.C. Li, Effect of characterizations of spacer in
823 electrodialysis cells on mass transfer, Desalination. 46 (1983) 243–252. doi:10.1016/0011-

824 9164(83)87161-6.

825